THE JOURNAL OF PHYSICAL CHEMISTRY B

Article

pubs.acs.org/JPCB

Virtual Synthesis of Thermally Cross-Linked Copolymers from a Novel Implementation of Polymatic

Lauren J. Abbott, Justin E. Hughes, and Coray M. Colina*

Department of Materials Science and Engineering, The Pennsylvania State University, University Park, Pennsylvania 16802, United States

Supporting Information

ABSTRACT: Because of the complex connectivity of cross-linked polymers, generating structures for molecular simulations is a nontrivial task. In this work, a general methodology is presented for constructing post-cross-linked polymers by a new two-stage implementation of the Polymatic simulated polymerization algorithm, where linear polymers are first polymerized and then cross-linked. It is illustrated here for an example system of thermally cross-linked octene−styrene−divinylbenzene (OS−DVB) copolymers. In the molecular models, the degree of cross-linking is ranged from 0 to 100%, and the resulting structural and thermal properties are examined. The simulations reveal an increase in the free volume with higher cross-linking degrees. Shifts in the peaks of the structure factors, which are assigned to contributions from the backbone and side-chain atoms, correspond to the formation of larger free volume elements. Furthermore, the glass transition temperatures increase with higher degrees of cross-linking, while the thermal expansivity decreases. Comparisons with experimental results for similar systems are made when available. As demonstrated here, the presented methodology will provide an effective route to simulating post-cross-linked polymers for a variety of applications, which will enable an improved understanding of their structure−property relationships.

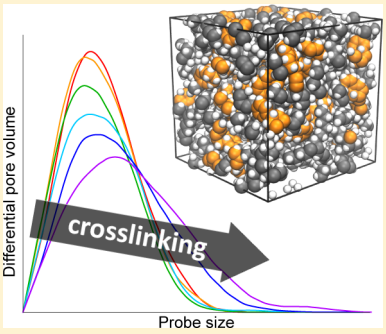

1. INTRODUCTION

The addition of cross-links to a polymer can have a large effect on its properties, generally providing good mechanical properties, high chemical and thermal stability, and low solubility. A variety of structures are possible via different cross-linking methods, and as a result, cross-linked polymers have found numerous applications as epoxy adhesives,[1] fuel cell membranes,[2,3] and self-healing materials,[4,5] among others. The post-cross-linking of polymers has been particularly useful in the design of porous polymers. For instance, a very high degree of cross-links can be incorporated into a polymer in the swollen state to provide a low-density structure with permanent porosity, termed hyper-cross-linked polymers (HCPs).[6] The tunability of the pore sizes by changing the structures and the degree of cross-linking makes these materials useful for applications such as gas storage,[7,8] gas separation,[9,10] and column chromatography.[11] Alternatively, thermal cross-linking has been exploited to enhance the properties of polymeric membranes for gas separations. While soluble, linear polymers can be readily cast into membranes, they can suffer from excessive swelling or plasticization, which diminishes their performance. Post-treatment of the polymeric membranes by thermal cross-linking has been shown to provide necessary rigidity to the system to suppress unwanted changes in the structure and maintain its properties.[12−14]

Molecular simulations have proven to be a useful tool in the study of network polymers due to the atomistic detail available, such that simulations have been used to provide an improved understanding of thermal, mechanical, structural, and adsorptive properties.[8,15−18] Recently, we have developed a predictive computational methodology for studying amorphous polymers, termed Polymatic,[19,20] which generates molecular models by a simulated polymerization approach. This methodology has been validated for a variety of glassy, linear polymers against a range of experimental data, including densities, X-ray scattering, glass transition temperatures, thermal expansion coefficients, and gas adsorption.[19,21,22] In addition, a similar approach was used to study an HCP, poly(dichloroxylene), by implementing the simulated polymerization to form the polymer chains and cross-links simultaneously, mimicking the experimental self-condensation reaction.[23] By controlling the amount of cross-links formed in the simulation, it was possible to explore the changes in porosity with increasing cross-linking degrees and predictively simulate gas adsorption isotherms consistent with experimental data.

In this work, we extend the application of Polymatic to study thermally cross-linked polymers by a two-stage implementation mimicking the synthetic process, where linear polymers are first polymerized and then post-cross-linked. This approach provides the most accurate description of the final network polymers by replicating an appropriate density of the linear polymers during the cross-linkg process. Here, we apply the technique to copolymers composed of 1-octene, styrene, and divinylbenzene (OS−DVB), as shown in Figure 1a, which were

Received: September 27, 2013
Revised: January 28, 2014
Published: January 29, 2014

   dx.doi.org/10.1021/jp409664d | J. Phys. Chem. B 2014, 118, 1916−1924

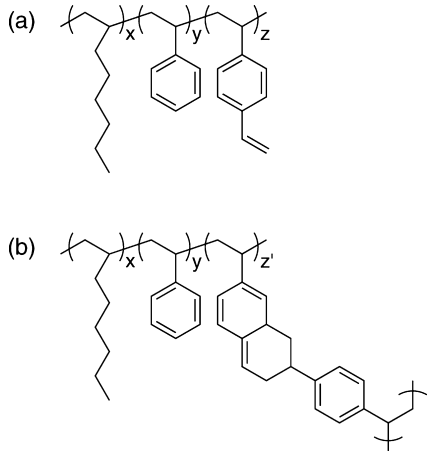

Figure 1. Chemical structures of (a) the linear OS−DVB copolymer containing 1-octene, styrene, and divinylbenzene, and (b) the cross-linked structure formed from a Diels−Alder [2 + 4] interchain cycloaddition reaction between two DVB units.

recently reported by Yuan and Chung.[24] In the experimental study, the linear polymers were subjected to a thermal cross-linking by a Diels−Alder [2 + 4] interchain cycloaddition reaction between neighboring DVB units, which results in a cross-linked system as illustrated in Figure 1b. Importantly, the resulting insoluble networks showed large absorption capacities for petroleum products, but the absorbency and swelling capacity were seen to be inversely proportional to the cross-linking degree, since a higher number of cross-links formed a more rigid network.

The organization of this work is as follows: In section 2, the simulation methods are given, including a detailed description of the structure generation procedure through a two-stage simulated polymerization. The results are then presented and discussed in section 3 upon variation of the cross-linking degree from 0 to 100%. In section 3.1, the free volume within the cross-linked OS−DVB copolymers is examined as well as the adsorption of several gases at moderate pressures. In section 3.2, the structure factors for the various cross-linking degrees are compared, and interpretation of the peaks is provided through analysis of the molecular models. In section 3.3, the thermal properties are explored, including the glass transition temperatures and thermal expansivity. Lastly, a few concluding remarks are provided in section 4.

2. SIMULATION METHODS

2.1. Models. Molecular models of the OS−DVB copolymers were described by the polymer consistent force field (PCFF).[25] For an accurate description of the electrostatics, partial charges for 1-octene and the cross-link unit were

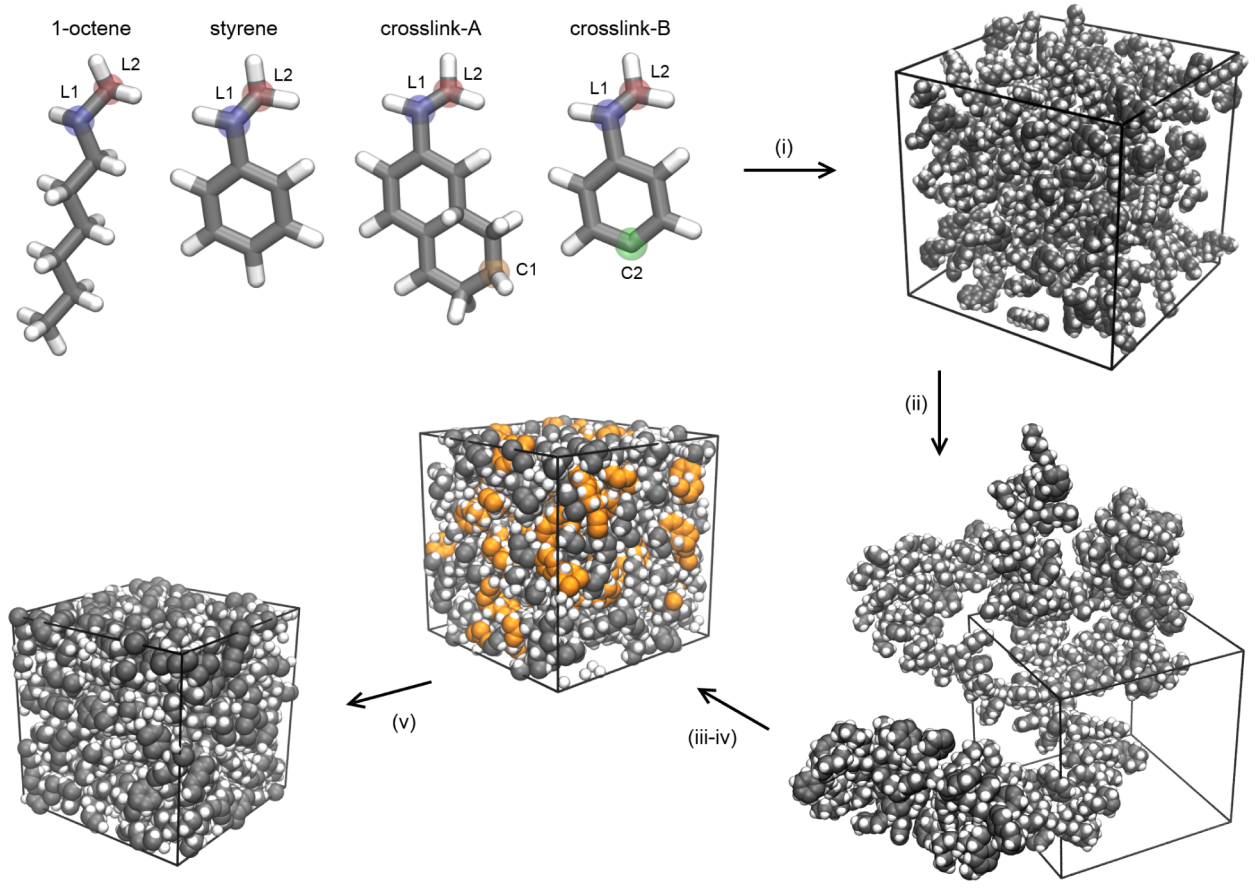

Figure 2. Representation of the structure generation procedure. (i) Random packing of the repeat units into a periodic simulation box. (ii) Simulated polymerization of linear polymers using Polymatic. The reactive atoms in this step are signified by "L1" and "L2" labels of the repeat units. (iii−iv) Compression to the cross-linking temperature, 513 K, and a simulated cross-linking to form a network using Polymatic. The reactive atoms in this step are signified by the "C1" and "C2" labels of the repeat units. The formed cross-linked units are highlighted in orange. (v) Compression to the final conditions of interest, 300 K and 1 bar.

dx.doi.org/10.1021/jp409664d | J. Phys. Chem. B 2014, 118, 1916−1924

obtained from *ab initio* calculations, while charges for the styrene unit were taken from previous work.[19] Note that charges were not calculated for the DVB monomers, but for the final cross-linked unit to provide the proper final structure (Figure 1b). The electrostatic potentials (ESP) were obtained at the HF/6-31G* level of theory in Gaussian 03,[26] and then a restrained electrostatic potential (RESP) charge fitting[27] was applied to calculate discrete partial charges. The atom types and partial charges for 1-octene and the cross-link unit are provided in Table S1 (Supporting Information).

Systems with various cross-linking degrees were studied, namely 0, 5, 25, 50, 75, and 100%. Here, the cross-linking degree was defined as the number percentage of repeat units in the polymer chain participating in a cross-link (i.e., the percentage of cross-link units), the notation for which is given by C-*X*, where *X* is the degree of cross-linking (e.g., C-50 corresponds to 50% cross-linking). It is important to note here that the two halves of the cross-link are considered as individual repeat units (cross-link-A and cross-link-B defined in Figure 2) in this determination. Each system has a total of 200 units, with the specified number of cross-link units corresponding to the theoretical cross-linking degree (half cross-link-A and half cross-link-B). The remaining units of the system were split among 1-octene and styrene such that a 81:19 ratio was maintained to be consistent with the previously reported experimental samples.[24] Upon completion of the simulated cross-linking, cross-link units that were not successfully cross-linked were replaced with styrene units, as described in the following section, leading to slightly lower actual cross-linking degrees. The composition of the initial linear polymers and final cross-linked systems are provided in Table 1.

Table 1. Compositions of Linear and Cross-Linked Polymers

	linear			cross-linked		
system	octene	styrene	cross-link	octene	styrene	cross-link
C-0	81	19	0	81	19	0
C-5	77	18	5	77	18.6	4.4
C-25	61	14	25	61	15.2	23.8
C-50	40.5	9.5	50	40.5	11.1	48.4
C-75	20.5	4.5	75	20.5	7.5	72
C-100	0	0	100	0	4.6	95.4

Compositions of the 1-octene, sytrene, and cross-link repeat units are presented as a number percentage of the total, averaged over five independent simulations. The cross-link percentages count each half of the cross-linking unit independently, with an equal amount of each cross-link-A and cross-link-B.

2.2. Structure Generation. Molecular models of the cross-linked OS−DVB copolymers were generated using the Polymatic simulated polymerization algorithm[19,20] and 21-step molecular dynamics compression scheme.[19,28] These methods have been validated for a variety of systems against available experimental data in previous work[19,21−23,28,29] and also have been shown to be effective for predictively screening amorphous materials not yet synthesized.[30,31] Here, the thermally cross-linked copolymers were generated with two stages of the simulated polymerization to mimic the actual synthesis, where linear polymers are first polymerized and then cross-linked. Since the final structures of cross-linked systems are known to be dependent on the conditions during cross-linking,[6,8] this two-stage approach is expected to provide the most accurate representation of the cross-linked polymers in this work. The structure generation procedure was performed in five steps: (i) initial packing of a periodic simulation box with repeat units, (ii) simulated polymerization of linear polymers, (iii) compression of the system to the cross-linking conditions, 513 K and 1 bar, (iv) simulated cross-linking, and (v) compression to 300 K and 1 bar, as illustrated in Figure 2.

Step 1: The specified number of each repeat unit corresponding to Table 1 (linear), totaling 200, was randomly packed into a simulation box under periodic boundary conditions at an initial density of 0.5 g cm^{-3} (step i in Figure 2). The repeat units were specified such that the proper polymerized structures would be obtained after the formation of bonds during the initial polymerization and following cross-linking stages. Note that the DVB units were not used but were replaced with two cross-linking units (half cross-link-A and half cross-link-B, as defined in Figure 2) to allow for a simplified cross-linking definition in the simulation for ease of implementation (described below). Since the cross-link units are similar to the DVB units, their replacement was not expected to have a significant impact on the final structures obtained.

Step 2: Linear polymers were obtained using a simulated polymerization, where repeat units in close proximity within the simulation box were bonded in between molecular dynamics steps (step ii in Figure 2). No distinction was made between repeat units during the polymerization, such that a random copolymer of the 1-octene, sytrene, and cross-link units was achieved. Specifically, a bond was formed between the closest pair of "L1" and "L2" atoms (as identified in the repeat units in Figure 2) within a cutoff distance of 6 Å. The algorithm was repeated until a single linear polymer of all 200 repeat units was obtained.

Step 3: The molecular models were equilibrated at 513 K and 1 bar (step iii in Figure 2), the conditions at which the OS−DVB copolymers were thermally cross-linked experimentally, to provide a proper initial structure for the cross-linking stage (described in step 4). This high-temperature state was achieved using a 21-step molecular dynamics compression scheme[19,28] with the following parameters: T_{final} = 513 K, T_{max} = 800 K, P_{final} = 1 bar, and P_{max} = 5 × 10^4 bar. In previous work,[19] this 21-step scheme was shown to predictively produce polystyrene at a range of conditions (temperature range of 294−469 K) with experimentally consistent densities, so it is expected to work equally well for the OS−DVB copolymers here. As such, use of the 21-step compression in this work is expected to yield realistic densities at the cross-linking conditions to provide an accurate representation of the experimental system during the cross-linking stage. Note that this step was not applied to the linear polymers (C-0), as no cross-linking was performed.

Step 4: The high-temperature linear polymers were cross-linked using a second stage of the simulated polymerization code (step iv in Figure 2). In order to simplify the cross-linking process in the simulations, cross-link units were defined to represent the final cross-linked structure, cross-link-A and cross-link-B in Figure 2, instead of the DVB unit. As such, during the cross-linking steps, bonds were made between the closest pair of "C1" and "C2" atoms (as indicated in the repeat units in Figure 2) within a cutoff distance of 6 Å. This simplified cross-linking enabled easier implementation of the simulated polymerization by requiring only the addition of a single bond and no change to the structure, unlike what would be required if the actual reaction process was mimicked. This modification was not expected to have a significant impact on

dx.doi.org/10.1021/jp409664d | J. Phys. Chem. B 2014, 118, 1916−1924

Table 2. Properties of Thermally Cross-Linked OS−DVB Copolymers[a]

polymer	ρ (g/cm^3)	FFV (%)	SA_{geom} (m^2/g)	N_{ads}, CH_4[b] (mmol/g)	q_{st}, CH_4[c] (kJ/mol)	T_g (K)	$\alpha_V \times 10^4$ [d] (1/K)
C-0	0.819 (0.008)	13.6 (0.8)	5 (2)	0.23 (0.06)	18.7	247	6.66
C-5	0.825 (0.007)	13.9 (0.7)	3 (2)	0.21 (0.07)	19.7	257	6.25
C-25	0.880 (0.005)	12.1 (0.5)	3 (1)	0.15 (0.04)	19.4	274	5.06
C-50	0.929 (0.01)	12.1 (1)	9 (11)	0.31 (0.08)	20.8	300	3.57
C-75	0.945 (0.007)	14.8 (0.6)	45 (23)	0.79 (0.1)	20.3	343	1.51
C-100	0.978 (0.01)	16.3 (1)	100 (47)	1.26 (0.1)	20.9	375	1.00

[a]Values are averaged over five simulations with standard deviations given in parentheses when available. [b]At 20 bar. [c]Extrapolated to zero coverage. [d]Taken at 300 K from the slope of the low-temperature region for the rubbery systems ($T_g \leq 300$ K) or the high-temperature region for the glassy systems ($T_g > 300$ K), according to Figure 7.

the final structures, since the cross-link units are similar to the DVB units. Any cross-link units remaining un-cross-linked after this step were replaced with styrene units, yielding the final polymer compositions given in Table 1 (cross-linked). Again, note that this step was not applied to the linear polymers (C-0).

Step 5: The final structures were subjected to the 21-step molecular dynamics compression scheme to achieve predicted final densities at standard temperature and pressure (step v in Figure 2). The parameters of the compression scheme in this stage were T_{final} = 300 K, T_{max} = 600 K, P_{final} = 1 bar, and P_{max} = 5 × 10^4 bar. This provided simulation models consistent with experimental samples for further characterization.

Each cross-linking degree was studied as the average of five independent structures, each generated using the process as described above. The final box sizes of the cross-linked systems were $L \approx 35$ Å. All energy minimization and molecular dynamics simulations during the Polymatic and 21-step compression stages were performed in the LAMMPS simulation package.[32] Molecular dynamics simulations utilized the velocity Verlet integrator with a 1 fs time step, and the canonical (NVT) and isothermal−isobaric (NPT) ensemble were controlled with a Nosé−Hoover thermostat and barostat. Nonbonded interactions were calculated with a cutoff of 15 Å, and long-range electrostatic interactions were described using the particle−particle particle−mesh (PPPM) method. Further details of the simulation methods are provided in the Supporting Information.

3. RESULTS AND DISCUSSION

The molecular models of the cross-linked OS−DVB copolymers were analyzed to explore the effect of the cross-linking degree (0−100%) on their properties, which are listed in Table 2. First, the free volume within the polymers is considered, as well as the adsorption of several gases at moderate pressures. Then, the structure factors from the simulations are examined, which can be considered a comparison to experimental X-ray scattering data. Interpretation of the peaks is provided utilizing the atomistic detail available in the simulations. Last, the thermal properties, including the glass transition temperatures and thermal expansivity, are discussed.

3.1. Free Volume. The free volume of the cross-linked OS−DVB copolymers was characterized using geometric measurements from the simulation models using the Poreblazer code.[33] The fractional free volume was determined from FFV = V_f/V_{sp}, where the free volume was calculated by $V_f = V_{sp} - 1.3V_w$ using geometric measures of the specific volume, V_{sp}, and van der Waals volume, V_w. In addition, geometric surface areas, SA_{geom}, were calculated using a spherical probe the size of a nitrogen molecule, since surface areas are typically derived experimentally through application of BET theory[34] to nitrogen adsorption isotherms at 77 K. These values for all systems are given in Table 2. Lastly, pore size distributions were calculated as the derivative of a void volume curve for increasing probe sizes, PSD = $-dV_{void}(D)/dD$, where $V_{void}(D)$ is the void volume accessible to a probe of diameter D. The PSDs for all systems are shown in Figure 3. Further discussion of these calculations can be found in the Supporting Information.

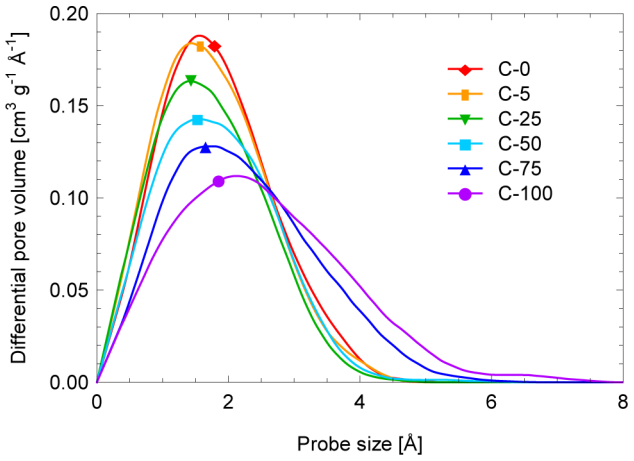

Figure 3. Differential pore volume present in the OS−DVB systems at 300 K with cross-linking degrees ranging from 0 to 100%.

Analysis of the free volume suggests that the OS−DVB copolymers with cross-linking degrees of 50% and below are essentially nonporous, while greater free volume was achieved in the C-75 and C-100 systems. In the lightly cross-linked systems, the free volume is smaller than the linear system, which suggests that the cross-links initially cause a slight collapse of the polymer chains. This can be seen by a decrease in the intensity of the PSD peak as the cross-linking is increased from 0 to 50%. Only in the C-75 and C-100 samples do the networks become rigid enough to form nontrivial free volume. For these polymers, the peaks in the PSDs shift slightly to larger values, but more importantly the breadths of the distributions have widened to include a greater proportion of larger free volume elements. The fractional free volumes and surface areas in these systems were therefore much larger than the systems with less cross-linking. We note that while the increase in free volume in these systems is partially due to the greater number of cross-links, the increased proportion of aromatic units is also likely to contribute (see Table 1). Importantly, on considering the size of gas molecules such as methane and nitrogen (>3.5 Å), only the C-75 and C-100 systems would be considered porous to the adsorption of these gases.

dx.doi.org/10.1021/jp409664d | J. Phys. Chem. B 2014, 118, 1916−1924

Similar correlations have been noted between porosity and the cross-linking degree in HCPs both experimentally[6,8,35,36] and in simulations.[23] Tsyurupa and Davankov,[6] for instance, observed a cross-linking degree (25−66%) at which a significant jump in the surface areas were observed in many HCP systems, usually from 0 to 60−200 m^2 g^{-1}. In our previous simulations of poly(DCX) HCPs, we saw comparable trends, where the porosity increased very little from 66 to 90% cross-linking (1 to 25 m^2 g^{-1}), but then improved substantially upon cross-linking to 122% (683 m^2 g^{-1}). These results are similar to those measured in the cross-linked OS−DVB copolymers here, where the systems remained essentially nonporous until greater than 50% cross-linking was imposed. While this work shows a similar rise in free volume upon increasing the cross-linking degree, it should be noted that the extent of the "porosity" available in these polymers is limited. This is likely due to the relatively high density at which the thermal cross-linking of the polymers is performed. The hyper-cross-linking of HCPs, on the other hand, occurs in a low-density, solvated state, and thus greater porosity is obtained in those materials.

In addition to the geometric measurements of the pore sizes, adsorption isotherms for the cross-linked copolymers were calculated for methane (CH_4), carbon dioxide (CO_2), nitrogen (N_2), and hydrogen (H_2) at 298 K by grand canonical Monte Carlo (GCMC) simulations in the MCCCS Towhee program.[37] Parameters for CH_4, CO_2, and N_2 were taken from the transferable potentials for phase equilibria (TraPPE),[38,39] while those for H_2 were taken from Darkrim and Levesque.[40] The average loading, N_{ads}, for all gases calculated from the simulations are given in Figure 4 and Figure S3, while the uptake of CH_4 at 20 bar is also given in Table 2. Comparison of the different cross-linking degrees reveals that significant loading was only observed in the C-75 and C-100 systems, as shown for CH_4 in Figure 4a, in agreement with the porosity calculations. However, their uptake is still quite low compared with other HCPs, even at moderate pressures. The isosteric heats of adsorption, q_{st}, calculated from the simulations (Figure S4, Table 2, and Table S2) are similar to those of comparable materials.[41−44] In general, q_{st} was slightly larger in the systems with greater cross-linking (≥50%), but a linear trend with cross-linking was not observed.

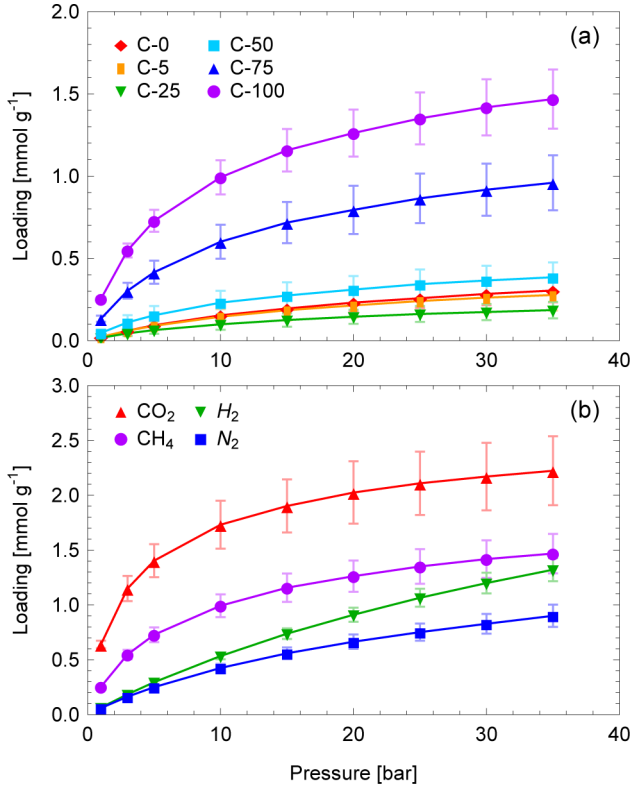

Figure 4. Adsorption isotherms at 298 K for (a) methane in the OS−DVB systems with 0−100% cross-linking and (b) methane, carbon dioxide, nitrogen, and hydrogen in the C-100 system.

At low pressures, the order of loading observed for the gases in each system was $CO_2 > CH_4 > H_2 > N_2$, which is illustrated for C-100 in Figure 4b. With the exception of H_2, this order follows the condensability of the gases given by their critical temperatures. For the polymers with lower free volume (≤50% cross-linking), the loading of H_2 was also larger than CH_4 at higher pressures. While H_2 has the lowest condensability, the greater adsorption of H_2 over N_2 and CH_4 in these cases is due to the very small sizes of pores available in the systems, as indicated by the PSDs in Figure 3. As such, the pore volume accessible to the smaller H_2 molecules (d_{H_2} = 2.875 Å) was significantly larger than that available to the larger N_2 and CH_4 molecules (d_{N_2} = 3.568 Å and d_{CH_4} = 3.817 Å).[45] This can be observed by the comparison of the pore volumes accessible to each gas given for all systems in Table S3, which were determined from the PSDs. For instance, while the pore volume in C-25 accessible to an H_2-size probe was 0.033 cm^3 g^{-1}, that for a CH_4-size probe was only 0.003 cm^3 g^{-1}.

3.2. Structure Factors. Additional structural characterization of the cross-linked OS−DVB copolymers was provided by structure factors, as given in Figure 5, which can be considered a comparison to experimental X-ray scattering data. The structure factors, $S(q)$, were taken as an average of the five boxes for each system at 300 K, calculated with the ISAACS program[46] as the Fourier transform of the radial distribution function, $g(r)$, which represents the probability of finding two atoms a distance r apart within the simulation model. The simulated structure factors have three peaks at low q (<4 $Å^{-1}$)

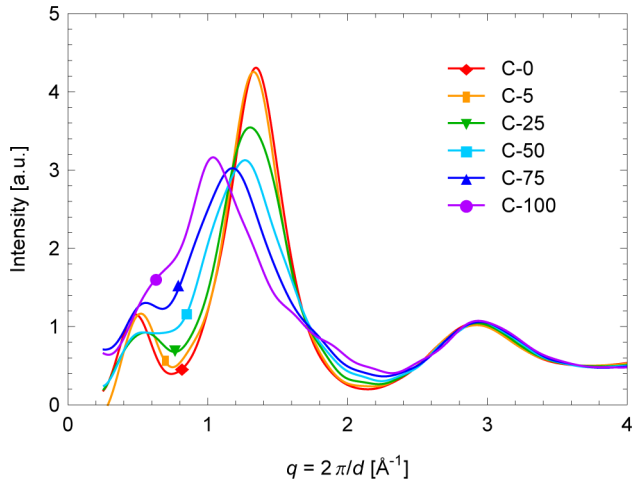

Figure 5. Total structure factors of the cross-linked OS−DVB systems with cross-linking degrees ranging from 0 to 100%. Results were averaged over five independent boxes; plots with error bars can be found in Figure S5.

dx.doi.org/10.1021/jp409664d | J. Phys. Chem. B 2014, 118, 1916−1924

and resemble the wide-angle X-ray scattering patterns of amorphous atactic polystyrene,[47] one component of the OS–DVB copolymers. The peak at the highest q (~3 Å^{-1} or ~2.1 Å), which corresponds to short distances on the order of bond lengths, does not change significantly between the different systems. The middle peak (~1.04–1.35 Å^{-1} or ~4.65–6.04 Å) initially decreases in intensity and then shifts to lower q with higher cross-linking. The position of the peak at the lowest q (~0.5–0.6 Å^{-1} or ~10.5–12.6 Å) does not change significantly between systems, and while its intensity changes some, it does not retain an order with the cross-linking degree. It is also important to note that this peak is not always as prominent and sometimes exists more as a shoulder in the structure factor, particularly in the systems with greater cross-linking.

The atomistic detail from the simulations was utilized to provide interpretation of the peaks in the structure factors. This was achieved by calculating partial structure factors, $S_{AB}(q)$, from partial radial distribution functions, $g_{AB}(r)$, defined by a scaled Faber–Ziman definition,[48] such that $S(q) = \sum_{A,B} S_{A,B}(q)$. This formulation has been utilized to provide interpretation to X-ray scattering data of PIMs[48] and OMIMs.[29] In this work, partial structure factors were calculated for the backbone–backbone, side-chain–side-chain, and backbone–side-chain interactions within the systems, as shown in Figure 6. The backbone atoms consist of the CH and CH_2 groups, while all other atoms constitute the side-chain atoms (Figure S6). If we consider first the linear C-0 system (Figure 6a), the backbone atoms appear to contribute fully to the peak at the lowest q (~0.5–0.6 Å^{-1}), while the side-chain atoms are responsible for the middle peak at ~1.04–1.35 Å^{-1}. Similar findings can be observed for the cross-linked systems, as shown for the C-50 system in Figure 6b (all systems in Figure S7). However, upon increasing the cross-linking degree, the side-chain atoms contribute increasingly to the lowest q peak, as well.

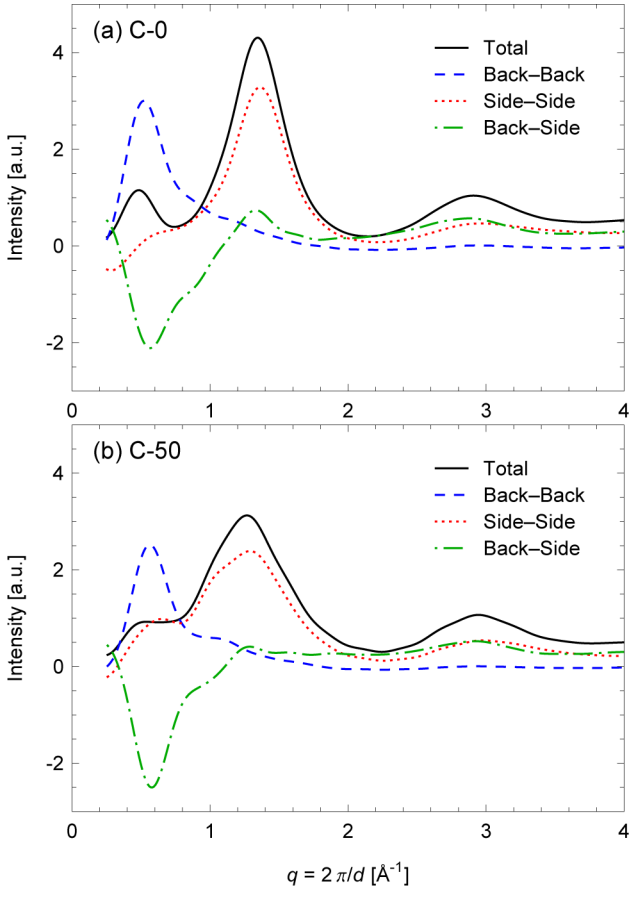

Figure 6. Partial structure factors split between the contributions of the backbone and side-chain atoms for the (a) C-0 and (b) C-50 systems.

Given the interpretations determined from the partial structure factors, connections can be made between the peaks in the structure factors and the free volume within the systems. In particular, we noted that the middle peak at ~1.04–1.35 Å^{-1} (~4.65–6.04 Å) resulted mainly from the side-chain atoms and shifted to slightly lower q with the higher cross-linking degrees. It can be concluded, therefore, that the increase in cross-linking held the side-chain atoms slightly further apart and generated larger free volume elements. A correlation can be drawn between the position of the middle peak in the structure factors with the average void size, $\bar{d}_{void}$, from the PSDs (Figure 3), which is given as the probe diameter at which half of the total void volume exists. For the systems with 50% cross-linking and less, $\bar{d}_{void}$ is about 1.75, which increases for the porous C-75 and C-100 systems up to 2.36 Å. These distances are shifted slightly from the peak positions of the structure factors by ~3 Å:

$$d_{peak} \approx \bar{d}_{void} + 3 \quad (1)$$

since the distances in the structure factors measure from the atom centers, while the PSDs yield distances excluding the volume occupied by the atoms. We will also note that the middle peak in the structure factors generally broadens with the greater cross-linking, which suggests that the random distribution of rigid spacers throughout the system creates a broader distribution of chain spacings. Correspondingly, the PSDs also broaden to cover a greater range of pore sizes.

The feature in the structure factors at the lowest q (~0.5–0.6 Å^{-1} or ~10.5–12.6 Å) was found to result from the backbone atoms. The separation distances between the chains are much larger than the free volume elements within the system, since the side-chains fill up that space. However, on comparison of the different cross-link degrees, we notice that the intensity of this peak in the structure factors seems to correlate most closely with the total amount of free volume in the system (Table 2). As such, the systems with the largest fractional free volume (C-75 and C-100) had the greatest intensity, while those with the smallest fractional free volume (C-25 and C-50) had the lowest intensity. Moreover, the breadth of this feature seems to widen with larger cross-linking degrees. In fact, for the systems with greater than 50% cross-linking, this feature appears as a shoulder in the structure factors, whereas it exists as a more prominent peak in the systems with lower cross-linking degrees. As we mentioned for the middle peak, the breath of this peak is likely correlated to the increasing amount of rigid cross-links, which provided a broader distribution of free volume elements in the system.

3.3. Thermal Properties. In order to study the thermal properties of the cross-linked OS–DVB copolymers, molecular dynamics simulations were performed in the NPT ensemble at 1 bar cooling stepwise (20 K every 500 ps) from a high temperature. The specific volume of the system as a function of temperature, averaged over the last 300 ps of each step, is shown in Figure 7. From this plot, the glass transition temperatures, T_g, can be obtained from the intersection of linear regressions applied to the low- and high-temperature

dx.doi.org/10.1021/jp409664d | J. Phys. Chem. B 2014, 118, 1916–1924

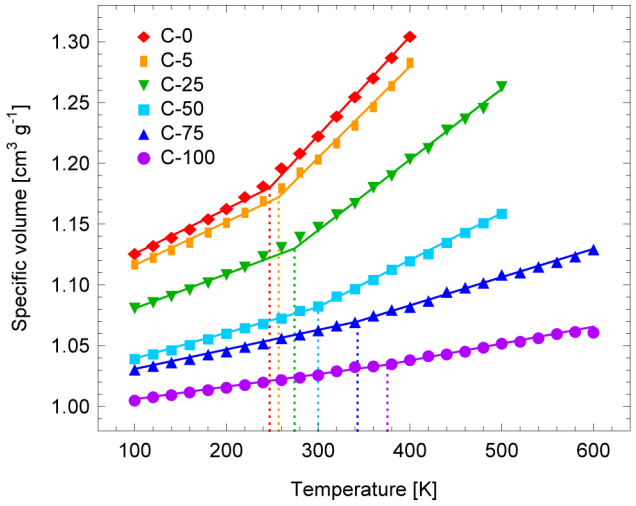

Figure 7. Specific volume of the cross-linked OS−DVB systems as a function of temperature, with cross-linking degrees ranging from 0 to 100%. Linear regressions for the low- and high-temperature regions are shown by the solid lines, while the glass transition temperatures are marked by the dashed vertical lines. Results were averaged over five independent boxes; plots with error bars can be found in Figure S8.

regions, which are illustrated by solid lines in Figure 7. The resulting T_g's are indicated by the dashed vertical lines, and their values are given in Table 2. As shown in Figure 8, T_g was

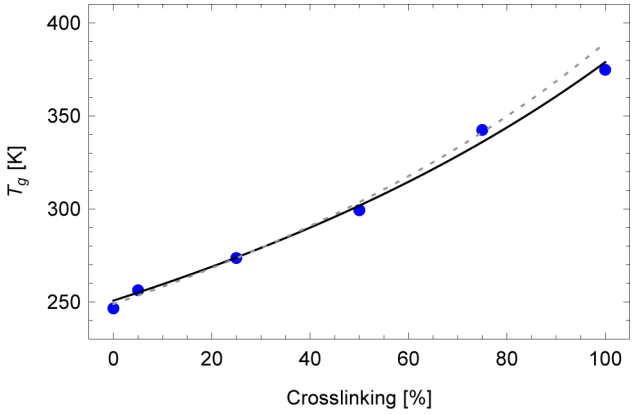

Figure 8. Glass transition temperature as a function of the degree of cross-linking. A best fit to the Gibbs−DiMarzio equation is also given when all systems were included in the fit (solid line) and when C-100 was excluded from the fit (dashed line).

seen to increase with the degree of cross-linking, consistent with the increased rigidity provided by the cross-links and the higher ratio of aromatic components. A best fit was found for the data using Gibbs−DiMarzio theory[49] with the equation

$$T_g = \frac{T_g^0}{1 - K_2 X} \tag{2}$$

as shown in Figure 8, where X is the degree of cross-linking, T_g^0 is the glass transition temperature of the un-cross-linked system, and K_2 is a constant. Determination of T_g was less distinctive for the higher cross-linking degrees (Figure S8), particularly the C-100 system, due to the high rigidity of the networks and the larger error bars in the simulations. Therefore, fits were performed with and without C-100, yielding parameters of T_g^0 = 250.7 K and K_2 = 0.338 (solid line) and T_g^0 = 248.9 K and K_2 = 0.361 (dashed line), respectively. In both cases, the agreement with the simulation data is good, and only small deviations are observed at the higher cross-linking degrees.

It is important to note that the glass transition temperatures calculated in the simulations are expected to be larger than what would be obtained experimentally due to the very fast cooling rates required in the simulations (in this work, cooling 20 K in just 500 ns). Despite this deviation, the proper trends are expected to hold.[19] It is possible to estimate an experimentally realistic T_g from the simulation values using the Williams−Landel−Ferry (WLF) equation, such that the deviation in temperature would be given by

$$\Delta T = \frac{-C_2 \log(t_{sim}/t_{exp})}{C_1 + \log(t_{sim}/t_{exp})} \tag{3}$$

where t_{sim} and t_{exp} are the cooling rates in the simulations and experiment, respectively.[50] Assuming the universal constants C_1 = 17.44 and C_2 = 51.6 K, as well as a typical experimental cooling rate of 20 K/min, the WLF equation yields $T'_g \approx T_g -$ 90 K. Therefore, the shifted T_g for the C-0 system, for instance, would be 157 K. Alternatively, the T_g of the linear copolymer C-0 can be estimated using the Fox equation by

$$\frac{1}{T_g} = \frac{w_A}{T_g^A} + \frac{w_B}{T_g^B} \tag{4}$$

where w_i and T_g^i are the weight fraction and glass transition temperature of component i. For the C-0 system, taking linear low-density polyethylene (w = 0.82 and T_g = 150 K) and polystyrene (w = 0.18 and T_g = 373 K),[51] the Fox equation estimates $T_g \approx$ 168 K, which is in good agreement with that determined using the WLF equation above.

In addition to the glass transition temperatures, the specific volume plot (Figure 7) also provides information about the volume expansion of the systems in response to the temperature changes. The thermal expansion coefficient at room temperature can be derived from the slope of the linear fits at 300 K as $\alpha_V = (1/V)(\partial V/\partial T)_P$, the values of which are given in Table 2. For the more lightly cross-linked systems, these expansion coefficients are similar to those of standard linear polymers, such as polystyrene and poly(methyl methacrylate) ($(1.7-3) \times 10^{-4}$ K^{-1}).[19] The thermal expansion coefficients of the OS−DVB copolymers were found to decrease (up to 6-fold) with the increasing cross-linking degree, as expected, due to the enhanced rigidity of the network. It is also important to note that for the C-75 and C-100 systems, the polymers became glassy at room temperature, accompanied by a significant change in the dynamics of the system and therefore lower expansivity. While the thermal expansion coefficient measures the response of the material to temperature, this parameter may give us some insight into the response to other external variables, such as the "swellability" of the material during the sorption of fluids. The trend observed in the simulations (less expansion as the degree of cross-linking was increased) is consistent with the experimental results reported for lightly cross-linked OS−DVB copolymers, where the swelling of the polymers upon absorption of oil decreased with larger cross-linking degrees.[24]

dx.doi.org/10.1021/jp409664d | J. Phys. Chem. B 2014, 118, 1916−1924

4. CONCLUSIONS

In this work, we presented a new approach for generating structures of cross-linked polymers in molecular simulations, where monomers were polymerized and post-cross-linked using the Polymatic simulated polymerization algorithm. The methodology was illustrated for a series of thermally cross-linked OS−DVB copolymers with cross-linking degrees ranging from 0 to 100%. The simulations illustrated the effects of the cross-linking on the structural and thermal properties, which were consistent with theory and experimental observations, and the available atomistic detail enabled an improved understanding of the structures of the cross-linked networks. Specifically, the change in free volume was examined as the degree of cross-linking was increased. Group contributions to the structure factors determined from the backbone and side-chain atoms in the simulations identified a relationship between the shift in the structure factor peaks with an increase in the size of the free volume elements. In addition, the increases in the degree of cross-linking corresponded to increased glass transition temperatures (247−375 K), in agreement with theory, and decreased thermal expansion coefficients. Overall, this work demonstrates the importance of the cross-linking degree on the resulting properties of networked polymers, such as the total free volume and rigidity, which are indicative of the potential of materials for gas adsorption applications. While the OS−DVB copolymers are given here as an example, the presented computational methodology and analysis will enable the effective study of other cross-linked polymeric materials for a variety of applications.

■ ASSOCIATED CONTENT

Supporting Information

Further details of simulation models and methods; adsorption isotherms; isosteric heats of adsorption; pore volumes for different probe sizes; total and partial structure factors; definition of backbone and side-chain atoms; specific volume versus temperature plots; complete ref 26. This material is available free of charge via the Internet at http://pubs.acs.org.

■ AUTHOR INFORMATION

Corresponding Author

*E-mail: colina@matse.psu.edu (C.M.C.).

Notes

The authors declare no competing financial interest.

■ ACKNOWLEDGMENTS

The authors thank T. C. Mike Chung for bringing the OS−DVB system to our attention. The authors also acknowledge the National Science Foundation (DMR-0908781 and DMR-1310258) for funding. Computational resources for this research were provided in part by the Materials Simulation Center of the Materials Research Institute, the Research Computing and Cyberinfrastructure unit of Penn State Information Technology Services, and the Penn State Center for Nanoscale Science. Additional computational resources were provided by instrumentation funded by the National Science Foundation (OCI-0821527).

■ REFERENCES

(1) Ratna, D. Modification of Epoxy Resins for Improvement of Adhesion: A Critical Review. *J. Adhes. Sci. Technol.* **2003**, *17*, 1655−1668.

(2) Hou, H.; Di Vona, M. L.; Knauth, P. Building Bridges: Crosslinking of Sulfonated Aromatic Polymers—A Review. *J. Membr. Sci.* **2012**, *423*−*424*, 113−127.

(3) Park, C. H.; Lee, C. H.; Guiver, M. D.; Lee, Y. M. Sulfonated Hydrocarbon Membranes for Medium-Temperature and Low-Humidity Proton Exchange Membrane Fuel Cells (PEMFCs). *Prog. Polym. Sci.* **2011**, *36*, 1443−1498.

(4) Chen, X.; Dam, M. A.; Ono, K.; Mal, A.; Shen, H.; Nutt, S. R.; Sheran, K.; Wudl, F. A Thermally Re-mendable Cross-Linked Polymeric Material. *Science* **2002**, *295*, 1698−1702.

(5) Wool, R. P. Self-Healing Materials: A Review. *Soft Matter* **2008**, *4*, 400−418.

(6) Tsyurupa, M. P.; Davankov, V. A. Porous Structure of Hypercrosslinked Polystyrene: State-of-the-Art Mini-Review. *React. Funct. Polym.* **2006**, *66*, 768−779.

(7) Germain, J.; Fréchet, J. M. J.; Svec, F. Hypercrosslinked Polyanilines with Nanoporous Structure and High Surface Area: Potential Adsorbents for Hydrogen Storage. *J. Mater. Chem.* **2007**, *17*, 4989−4997.

(8) Wood, C. D.; Tan, B.; Trewin, A.; Niu, H.; Bradshaw, D.; Rosseinsky, M. J.; Khimyak, Y. Z.; Campbell, N. L.; Kirk, R.; Stöckel, E.; Cooper, A. I. Hydrogen Storage in Microporous Hypercrosslinked Organic Polymer Networks. *Chem. Mater.* **2007**, *19*, 2034−2048.

(9) Germain, J.; Fréchet, J. M. J.; Svec, F. Nanoporous, Hypercrosslinked Polypyrroles: Effect of Crosslinking Moiety on Pore Size and Selective Gas Adsorption. *Chem. Commun.* **2009**, *12*, 1526−1528.

(10) Luo, Y.; Li, B.; Wang, W.; Wu, K.; Tan, B. Hypercrosslinked Aromatic Heterocyclic Microporous Polymers: A New Class of Highly Selective CO_2 Capturing Materials. *Adv. Mater.* **2012**, *24*, 5703−5707.

(11) Urban, J.; Svec, F.; Fréchet, J. M. J. Hypercrosslinking: New Approach to Porous Polymer Monolithic Capillary Columns with Large Surface Area for the Highly Efficient Separation of Small Molecules. *J. Chromatogr., A* **2010**, *1217*, 8212−8221.

(12) Kratochvil, A. M.; Koros, W. J. Decarboxylation-Induced Cross-Linking of a Polyimide for Enhanced CO_2 Plasticization Resistance. *Macromolecules* **2008**, *41*, 7920−7927.

(13) Du, N.; Dal-Cin, M. M.; Pinnau, I.; Nicalek, A.; Robertson, G. P.; Guiver, M. D. Azide-based Cross-Linking of Polymers of Intrinsic Microporosity (PIMs) for Condensable Gas Separation. *Macromol. Rapid Commun.* **2011**, *32*, 631−636.

(14) Li, F. Y.; Xiao, Y.; Chung, T.-S.; Kawi, S. High-Performance Thermally Self-Cross-Linked Polymer of Intrinsic Microporosity (PIM-1) Membranes for Energy Development. *Macromolecules* **2012**, *45*, 1427−1437.

(15) Liu, J. W.; Mackay, M. E.; Duxbury, P. M. Molecular Dynamics Simulation of Intramolecular Cross-Linking of BCB/Styrene Copolymers. *Macromolecules* **2009**, *42*, 8534−8542.

(16) Hörstermann, H.; Hentschke, R.; Amkreutz, M.; Hoffmann, M.; Wirts-Rütters, M. Predicting Water Sorption and Volume Swelling in Dense Polymer Systems via Computer Simulation. *J. Phys. Chem. B* **2010**, *114*, 17013−17024.

(17) Li, C.; Strachan, A. Molecular Dynamics Predictions of Thermal and Mechanical Properties of Thermoset Polymer EPON862/DETDA. *Polymer* **2011**, *52*, 2920−2928.

(18) Shenogina, N. B.; Tsige, M.; Patnaik, S. S.; Mukhopadhyay, S. M. Molecular Modeling Approach to Prediction of Thermo-mechanical Behavior of Thermoset Polymer Networks. *Macromolecules* **2012**, *45*, 5307−5315.

(19) Abbott, L. J.; Hart, K. E.; Colina, C. M. Polymatic: A Generalized Simulated Polymerization Algorithm for Amorphous Polymers. *Theor. Chem. Acc.* **2013**, *132*, 1334.

(20) Abbott, L. J. Polymatic: A Simulated Polymerization Algorithm, Version 1.0; 2013; http://nanohub.org/resources/17278.

(21) Hart, K. E.; Abbott, L. J.; Colina, C. M. Analysis of Force Fields and BET Theory for Polymers of Intrinsic Microporosity. *Mol. Simul.* **2013**, *39*, 397−404.

(22) Zhou, X.; Li, Y.; Hart, K. E.; Abbott, L. J.; Lin, Z.; Svec, F.; Colina, C. M.; Turner, S. R. Nanoporous Structure of Semirigid

Alternating Copolymers via Nitrogen Sorption and Molecular Simulations. *Macromolecules* **2013**, *46*, 5968−5973.
(23) Abbott, L. J.; Colina, C. M. Atomistic Structure Generation and Gas Adsorption Simulations of Microporous Polymer Networks. *Macromolecules* **2011**, *44*, 4511−4519.
(24) Yuan, X.; Chung, T. C. M. Novel Solution to Oil Spill Recovery: Using Thermodegradable Polyolefin Oil Superabsorbent Polymer (Oil-SAP). *Energy Fuels* **2012**, *26*, 4896−4902.
(25) Sun, H. Force Field for Computation of Conformational Energies, Structures, and Vibrational Frequencies of Aromatic Polyesters. *J. Comput. Chem.* **1994**, *15*, 752−768.
(26) Frisch, M. J.; Trucks, G. W.; Schlegel, H. B.; Scuseria, G. E.; Robb, M. A.; Cheeseman, J. R.; Montgomery, J. A., Jr.; Vreven, T.; Kudin, K. N.; Burant, J. C.; et al. *Gaussian 03, Revision C.02*; Gaussian Inc: Wallingford, CT, 2004.
(27) Bayly, C. I.; Cieplak, P.; Cornell, W.; Kollman, P. A. A Well-Behaved Electrostatic Potential Based Method Using Charge Restraints for Deriving Atomic Charges: The RESP Model. *J. Phys. Chem.* **1993**, *97*, 10269−10280.
(28) Larsen, G. S.; Lin, P.; Hart, K. E.; Colina, C. M. Molecular Simulations of PIM-1-like Polymers of Intrinsic Microporosity. *Macromolecules* **2011**, *44*, 6944−6951.
(29) Abbott, L. J.; McDermott, A. G.; Del Regno, A.; Taylor, R. G. D.; Bezzu, C. G.; Msayib, K. J.; McKeown, N. B.; Siperstein, F. R.; Runt, J.; Colina, C. M. Characterizing the Structure of Organic Molecules of Intrinsic Microporosity by Molecular Simulations and X-ray Scattering. *J. Phys. Chem. B* **2013**, *117*, 355−364.
(30) Hart, K. E.; Abbott, L. J.; McKeown, N. B.; Colina, C. M. Toward Effective CO_2/CH_4 Separations by Sulfur-Containing PIMs via Predictive Molecular Simulations. *Macromolecules* **2013**, *46*, 5371−5380.
(31) Abbott, L. J.; McKeown, N. B.; Colina, C. M. Design Principles for Microporous Organic Solids from Predictive Computational Screening. *J. Mater. Chem. A* **2013**, *1*, 11950−11960.
(32) Plimpton, S. Fast Parallel Algorithms for Short-Range Molecular Dynamics. *J. Comput. Phys.* **1995**, *117*, 1−19.
(33) Sarkisov, L.; Harrison, A. Computational Structure Characterisation Tools in Application to Ordered and Disordered Porous Materials. *Mol. Simul.* **2011**, *37*, 1248−1257.
(34) Brunauer, S.; Emmett, P. H.; Teller, E. Adsorption of Gases in Multimolecular Layers. *J. Am. Chem. Soc.* **1938**, *60*, 309−319.
(35) Zeng, S.-Z.; Guo, L.; He, Q.; Chen, Y.; Jiang, P.; Shi, J. Facile One-Pot Synthesis of Nanoporous Hypercrosslinked Hydroxybenzene Formaldehyde Resins with High Surface Area and Adjustable Pore Texture. *Microporous Mesoporous Mater.* **2010**, *131*, 141−147.
(36) Li, B.; Gong, R.; Wang, W.; Huang, X.; Zhang, W.; Li, H.; Hu, C.; Tan, B. A New Strategy to Microporous Polymers: Knitting Rigid Aromatic Building Blocks by External Cross-Linker. *Macromolecules* **2011**, *44*, 2410−2414.
(37) Martin, M. G. Monte Carlo for Complex Chemical Systems (MCCCS) Towhee, Version 7.0.4; 2010; http://towhee.sourceforge.net.
(38) Martin, M. G.; Siepmann, J. I. Transferable Potentials for Phase Equilibria. 1. United-Atom Description of *n*-Alkanes. *J. Phys. Chem. B* **1998**, *102*, 2569−2577.
(39) Potoff, J. J.; Siepmann, J. I. Vapor−Liquid Equilibria of Mixtures Containing Alkanes, Carbon Dioxide, and Nitrogen. *AIChE J.* **2001**, *47*, 1676−1682.
(40) Darkrim, F.; Levesque, D. Monte Carlo Simulations of Hydrogen Adsorption in Single-Walled Carbon Nanotubes. *J. Chem. Phys.* **1998**, *109*, 4981−4984.
(41) Germain, J.; Fréchet, J. M. J.; Svec, F. Nanoporous Polymers for Hydrogen Storage. *Small* **2009**, *5*, 1098−1111.
(42) Dawson, R.; Stöckel, E.; Holst, J. R.; Adams, D. J.; Cooper, A. I. Microporous Organic Polymers for Carbon Dioxide Capture. *Energy Environ. Sci.* **2011**, *4*, 4239−4245.
(43) Moellmer, J.; Moeller, A.; Dreisbach, F.; Glaeser, R.; Staudt, R. High Pressure Adsorption of Hydrogen, Nitrogen, Carbon Dioxide and Methane on the Metal−Organic Framework HKUST-1. *Microporous Mesoporous Mater.* **2011**, *138*, 140−148.
(44) Qiao, S.; Du, Z.; Yang, R. Design and Synthesis of Novel Carbazole−Spacer−Carbazole Type Conjugated Microporous Networks for Gas Storage and Separation. *J. Mater. Chem. A* **2014**, *2*, 1877−1885.
(45) Robeson, L. M.; Freeman, B. D.; Paul, D. R.; Rowe, B. W. An Empirical Correlation of Gas Permeability and Permselectivity in Polymers and Its Theoretical Basis. *J. Membr. Sci.* **2009**, *341*, 178−185.
(46) Le Roux, S.; Petkov, V. ISAACS—Interactive Structure Analysis of Amorphous and Crystalline Systems. *J. Appl. Crystallogr.* **2010**, *43*, 181−185.
(47) Mitchell, G. R.; Windle, A. H. Structure of Polystyrene Glasses. *Polymer* **1984**, *25*, 906−920.
(48) McDermott, A. G.; Larsen, G. S.; Budd, P. M.; Colina, C. M.; Runt, J. Structural Characterization of a Polymer of Intrinsic Microporosity: X-ray Scattering with Interpretation Enhanced by Molecular Dynamics Simulations. *Macromolecules* **2011**, *44*, 14−16.
(49) DiMarzio, E. A. On the Second-Order Transition of a Rubber. *J. Res. Natl. Bur. Stand., Sect. A* **1964**, *68A*, 611−617.
(50) Soldera, A.; Metatla, N. Glass Transition of Polymers: Atomistic Simulation Versus Experiments. *Phys. Rev. E* **2006**, *74*, 061803.
(51) Mark, J. E., Ed.; *Polymer Data Handbook*, 2nd ed.; Oxford University Press: New York, 2009.